Direct Laser Writing of 3D Architectures of Aligned Carbon Nanotubes

Shota Ushiba, Satoru Shoji, Kyoko Masui, Junichiro Kono, and Satoshi Kawata*

Carbon nanotubes (CNTs) exhibit ultrahigh aspect ratios that can lead to devices and systems with extremely anisotropic mechanical,[1] electrical,[2] thermal,[3,4] and optical properties[5] if a macroscopic ensemble of aligned CNTs can be made. There have been reports on methods for obtaining macroscopically aligned CNTs on substrates,[6,7] or in simple structures such as fibers,[8,9] and films,[10,11] which have led to successful demonstrations of aligned CNTs as photodetectors,[12] polarizers,[5,13] actuators,[14] and metamaterials.[15] However, it still remains to be a significant challenge to control the orientation direction of CNTs in three-dimensional (3D) architectures.

Here, we use direct laser writing through two-photon polymerization (TPP) lithography to fabricate 3D nanostructures containing aligned single-wall CNTs (SWCNTs). Direct laser writing, based on a femtosecond-laser based nanofabrication technique, has been established as a powerful tool for fabrication and integration of arbitrary 3D micro/nano polymer objects.[16,17] Some progress has been also made recently with fabrication of structures with sub-100 nm feature sizes, which is attained by employing a stimulated emission depletion (STED) technique.[18,19] A near-infrared femtosecond pulsed laser beam is focused on an UV-curable monomer, resulting in solidification of a nanometric volume of the monomer in the focus spot through two-photon absorption.[20,21] Arbitrary structures can be created by 3D scanning of the focus spot. This technique has opened up a wide range of applications, including photonic crystals,[22] photonic quasicrystals,[23] metamaterials,[24] mechanical metamaterials,[25] and functional micro-/nano-mechanical devices.[26] TPP lithography is also an ideal tool for developing composites made of polymer and nanomaterials. There have already been some reports of nanocomposites, including photoisomerizable dyes,[27] semiconductor nanoparticles,[28] metallic nanoparticles,[29] and magnetic nanoparticles.[30]

Our approach, based on TPP lithography, enables fabrication of arbitrarily complicated and fine 3D structures containing SWCNTs. SWCNTs in a nanowire fabricated by this TPP lithography technique are aligned along the wire,[31] which enables to align SWCNTs in any desired spatial directions, thus opening up a variety of new possibilities of fabricating complex 3D architectures that are made of aligned SWCNTs.

To make SWCNT/polymer composites, we loaded a 0.01 wt% solution of SWCNTs into an UV-curable monomer (see *Samples* in the Experimental Section). TPP lithography was carried out on the SWCNT-dispersed photo-resin, and SWCNTs were simultaneously fixed in tiny polymer structures (**Figure 1**a). After the structures were created, unsolidified resin was rinsed away using acetone, and the structures were then dried. 3D structures as well as suspended nanowires were fabricated with feature resolution far beyond the diffraction limit of light, in which SWCNTs were indeed embedded (Figure 1b–d). The orientation direction and degree of the alignment of SWCNTs in the obtained structures were investigated using polarized Raman microspectroscopy (see Experimental Section for more details).

To provide insight into how the strength of alignment changes as the nanowire becomes narrower, we fabricated a series of nanowires with different widths. **Figure 2**a presents Raman spectra of a 375 nm wide nanowire (Figure 1b,c), taken at different angles θ between the polarization of the incident laser beam and the nanowire axis. Both the G-band (1590 cm^{-1}) and D-band (1350 cm^{-1}) peaks significantly vary in intensity as a function of θ. The angular dependence of the G-band intensity, $I_G(\theta)$, is polar-plotted and fitted with Equation 1 (see Figure 2b and Experimental Section). The plot shows that the G-band intensity becomes largest when the polarization of the incident laser beam is parallel to the nanowire axis ($\theta \approx 0$ and 180°), while the intensity becomes smallest when the polarization is perpendicular ($\theta \approx 90$ and 270°). The result clearly indicates that SWCNTs are strongly aligned inside the wire, as illustrated in Figure 2c. There were no SWCNTs stuck on the nanowire surface, as confirmed by the SEM images, that is, SWCNTs are aligned inside the nanowire. From the fitting curve, the nematic order parameter, S,[31,32] which represents the strength of alignment, is calculated to be 0.4. **Figure 3**a displays SEM images of the fabricated nanowires, whose widths are 375, 425, 490, 540, 675, 840, and 995 nm, respectively. The angular dependence for each wire is measured, and S is plotted as a function of width in Figure 3b. S is found to increase with decreasing wire width. Indeed, S for the 375 nm wide nanowire is twice as large as that for the 995 nm wide nanowire. This result gives a clear indication that SWCNTs are more strongly aligned in thinner nanowires.

Based on these inspiring results, we fabricated more complex 3D structures consisting of arrays of nanowires containing aligned CNTs. **Figure 4**a and b show SEM images of a 3D structure with a size of 3 μm × 3 μm × 4 μm, which is composed of arrays of 16 nanowires stacked in 11 layers (Figure 4c,d).

S. Ushiba, Dr. S. Shoji,[+] Dr. K. Masui, Prof. S. Kawata
Department of Applied Physics
Osaka University
2-1 Yamadaoka, Suita, Osaka 565-0871, Japan
Prof. J. Kono
Department of Electrical and Computer Engineering
Rice University
Houston, Texas 77005, USA
[+]Present address: Department of Engineering Science, The University of Electro-Communications, 1-5-1 Chofugaoka, Chofu, Tokyo, 182-8585, Japan

DOI: 10.1002/adma.201400783

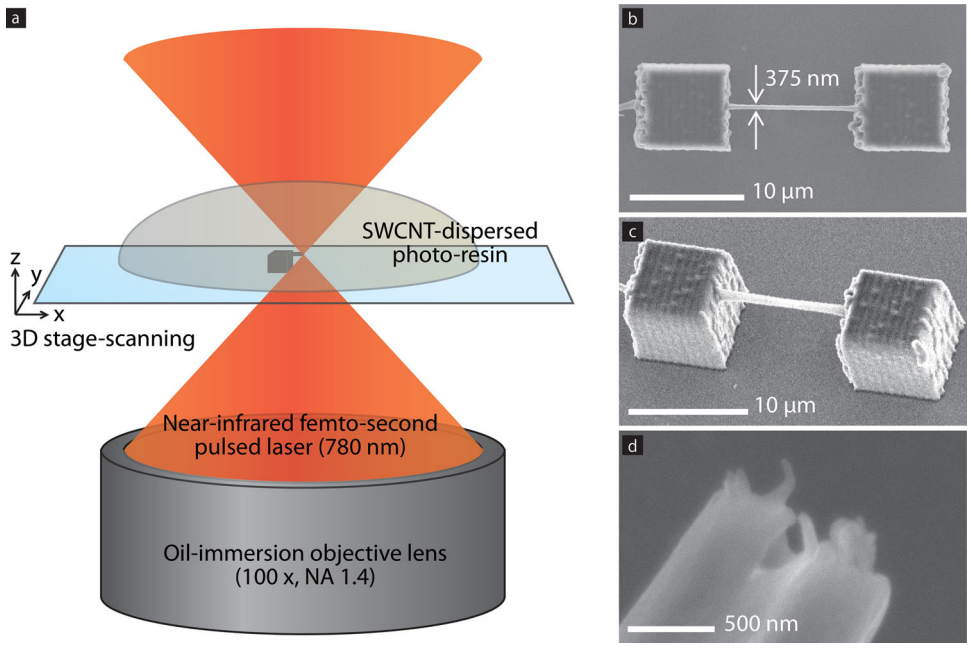

Figure 1. 3D fabrication of SWCNT/polymer composites by TPP lithography. a) Schematic showing 3D microfabrication of SWCNT/polymer composites based on TPP lithography. Femtosecond pulsed laser beam (780 nm) is focused on SWCNT-dispersed photo-resin through an oil-immersion objective lens (100x, NA 1.4). The focus spot is three dimensionally moved relative to the stage, and the composites are created following the trajectory of the focus spot. b,c) SEM images of a 375 nm wide, 10 μm long nanowire, suspended between two microboxes, ca. 7 μm above the substrate. (b) and (c) are top and perspective views, respectively. d) SEM image of a cross-section of the nanowire, showing that SWCNTs are embedded inside.

The width of each nanowire in the structure is around 530 nm. The polarization dependence of the Raman G-peak, $I_G(\theta)$, is polar-plotted in Figure 4e, which gives a clear indication that SWCNTs are aligned even in this 3D structure. The orientation direction is along the scanning direction, namely, parallel to nanowires. From the fitting curve, S is calculated to be 0.2. It is interesting to note that S for the box (0.2) is smaller than that for the suspended nanowire (0.3), even though the wire width is the same. This means that the strength of the alignment is affected by structural shape.

Finally, we demonstrate that the orientation direction is controlled in a 3D structure by changing the laser scanning direction. **Figure 5**a and b show SEM images of a single microstructure with dimensions of 3 μm × 6 μm × 4 μm. This structure is separated into two sections in which the laser scanning directions are orthogonal to each other; the left section is made up of an array of nanowires along the x-axis, while the right section is made up of an array of nanowires along the y-axis (Figure 5c and d). The polarization of the fabrication laser beam was kept parallel to the x-axis regardless of the scanning direction. The angular dependence, $I_G(\theta)$, where θ is now defined as the angle between the laser polarization and the x-axis, for the two sections is polar-plotted in Figure 5e, which clearly shows that SWCNTs are oriented in the scanning direction in each

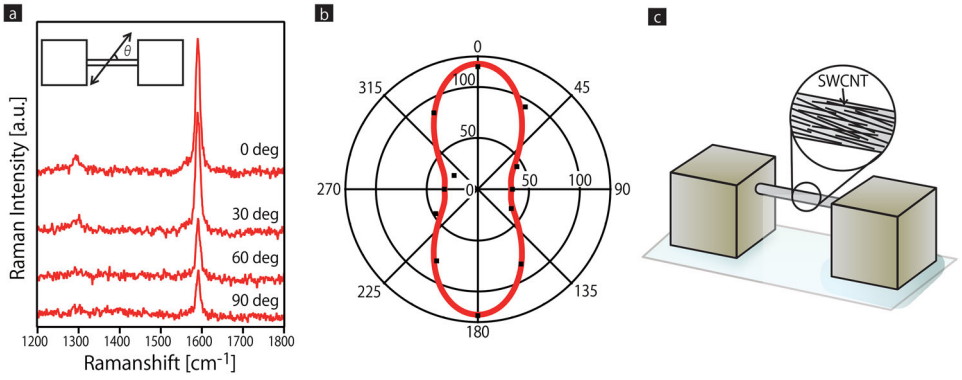

Figure 2. Alignment characterization of SWCNTs in a nanowire with polarized Raman microspectroscopy. a) Raman spectra taken at different polarization angles, $\theta = 0, 30, 60, 90°$, that are defined as the angle between the polarization of the incident laser beam and the wire axis, as shown in the inset. The excitation wavelength, laser power, and exposure time for the Raman measurements were 785 nm, 0.96 mW and 5 s, respectively. b) Polar diagram showing the G-band intensity as a function of θ, revealing that the SWCNTs inside the wire are orientated along the wire axis. The dots representing experimental results are fitted with Equation 1. c) Illustration that represents alignment of SWCNTs along the wire axis.

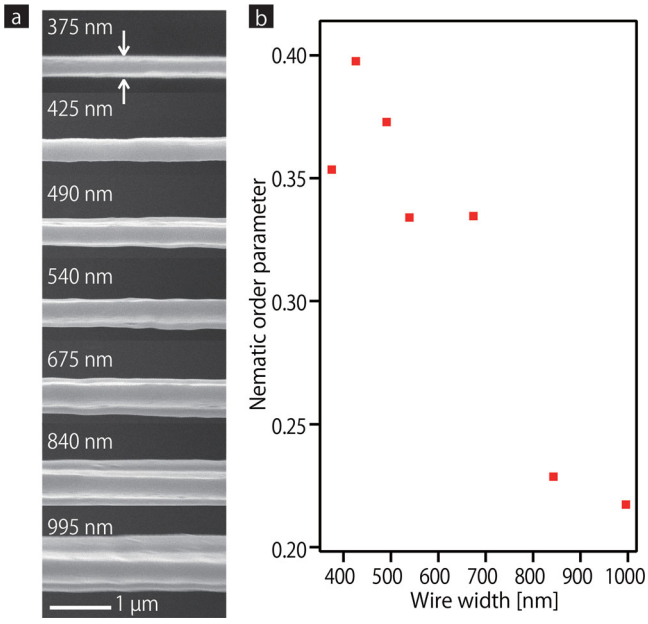

Figure 3. Strength changes of the alignment of SWCNTs as a function of wire width. a) Series of SEM images of suspended nanowires, whose wire widths are 375, 425, 490, 540, 675, 840, and 995 nm, respectively. b) The nematic order parameter, *S*, as a function of wire width, for the wires shown in (a), measured through polarization-dependent Raman spectroscopy.

section. It is interesting to note that *S* of the *x*-scanning area (0.2) is twice greater than that in the *y*-scanning area (0.1). The result implies that the polarization of the fabrication laser beam affected the strength of the alignment in the structure.

On the basis of the obtained results, we suggest that the alignment mechanism involves three factors: i) spatial confinement, ii) volume shrinkage, and iii) optical gradient forces. SWCNTs are spatially confined in nanowires because the typical length of SWCNTs we used was longer than the nanowire widths, which resulted in alignment along the wire (i.e., the laser scanning direction). However, as the nanowire becomes wider, SWCNTs are not strictly confined in space, resulting in weaker alignment, as observed in Figure 3b. The alignment is further enhanced by volume shrinkage of structures arising from extraction of unsolidified resin remaining in the structures during rinse and dry process.[34] The shrinkage results in tensile force on the nanowire, also leading to alignment. However, the shrinkage rate becomes close to 0% with increasing dimensions,[34] and thus the degree of alignment drops in the wider wires as well as in 3D structures, as observed in our experimental results. Moreover, optical gradient force also contributes to the alignment during the fabrication as the gradient force makes 1D nanostructures align along the polarization direction.[35,36] This is consistent with the result in Figure 5b, which shows that SWCNTs are more strongly aligned in the section where the polarization is parallel to the scanning direction. All these three mechanisms contribute to the alignment of SWCNTs during TPP lithography.

In conclusion, we have developed a technique based on TPP lithography to fabricate arbitrary 3D structures in which aligned SWCNTs are embedded. SWCNTs are aligned along nanowires or laser scanning directions while they are embedded in the structure, as evidenced by polarized Raman microspectroscopy. The alignment is induced by spatial confinement, volume shrinkage, and optical gradient force. The obtained composites, which exhibit the nematic order parameters up to 0.4, should lead to an enhancement of mechanical,[1] electrical,[2] thermal,[3,4] and optical properties,[5] as anisotropic properties resemble those of individual SWCNTs, thereby opening up possibilities of making devices and systems consisting of macroscopic ensembles of aligned SWCNT. Our method can also attain vertical alignment of SWCNTs if the laser is scanned along vertical direction. Further, the alignment along vertical direction would be also enhanced with tailoring polarization of the laser beam parallel to *z*-direction that is created by focusing radially polarized laser beam. Our method, thus, enables

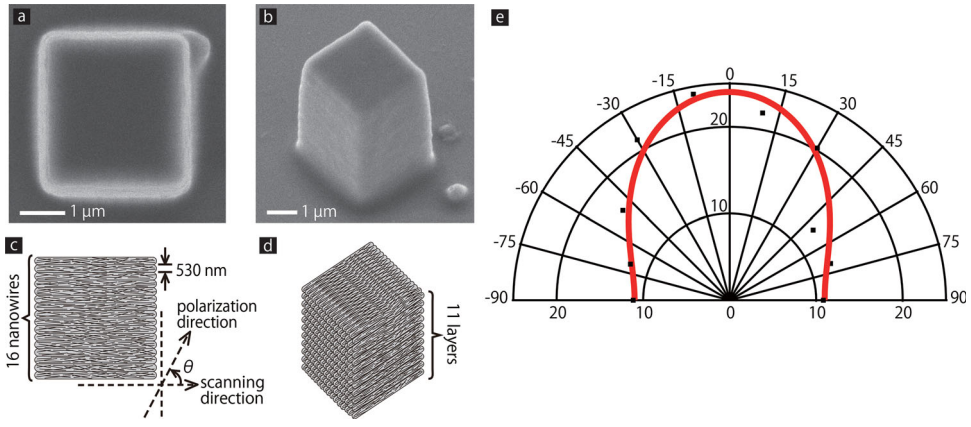

Figure 4. Uniaxial alignment of SWCNTs in a 3D structure made of an array of nanowires. a,b) SEM images of a 3D structure that is made of arrays of nanowires with a size of 3 μm × 3 μm × 4 μm. (a) and (b) are top and perspective views, respectively. c,d) Schematic images showing that the structure is made up of an array of 16 nanowires stacked in 11 layers. (c) and (d) are top and perspective views, respectively. e) Polar-diagram showing the G-band intensity as a function of the angle θ between the polarization of the incident laser beam and the scanning direction. The excitation wavelength, laser power, and exposure time for the Raman measurements were 785 nm, 3.3 mW, and 5 s, respectively. The dots representing experimental results are fitted with Equation 1.

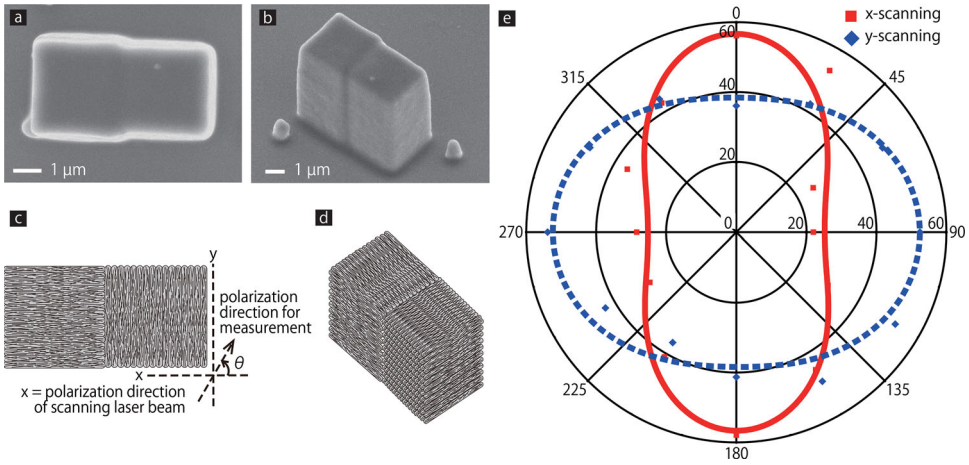

Figure 5. Alignment manipulation of SWCNTs in a single microstructure. a,b) SEM images of a single microstructure that is composed of two sections. The left section is made up of an array of nanowires along *x*-axis, while the right section is made up of an array of nanowires along *y*-axis. The coordinate is defined in (c). (a) and (b) are top and perspective views, respectively. c,d) Schematic images showing that the structure is made up of arrays of nanowires in two different orientations. The inset defines the coordinate, and θ is defined as the angle between the polarization of the incident laser beam and the *x*-axis. (a) and (b) are top and perspective views, respectively. e) Polar-diagram showing the G-band intensity as a function of the angle θ representing that SWCNTs are oriented along the scanning direction. The square and diamond symbols represent the angular dependence in the *x*-scanning area and *y*-scanning area, respectively. Both are fitted with Equation 1. The excitation wavelength, laser power, and exposure time for the Raman measurements were 785 nm, 3.3 mW, and 7 s, respectively.

alignment control in any desired directions in arbitrary 3D nanostructures, which should lead to new applications such as actuators[14] and metamaterials.[15]

Experimental Section

Samples: SWCNTs (HiPco Single-Wall Carbon Nanotubes, Unidym) were used in this study. The diameter and the length of SWCNTs we used in this study are in the range of 0.8 to 1.2 nm, and 100 to 1000 nm, respectively. A 0.01 wt% solution of SWCNTs was loaded into an acrylate monomer, R712, provided from Nippon Kayaku Co. Ltd., and dispersed using a sonicatior (250D-advanced, model # 101–063–837, Branson) for 1 h. This concentration is an optimized value to fabricate fine microstructures without large aggregated SWCNTs.[31] Photo-initiator (Benzil, Wako) and photo-sensitizer (2-benzyl-2-(dimethylamino)-4′-morpholinobutyrophenon, Aldrich) were subsequently mixed into the resin to be at a ratio of 1.67 wt% and 1.67 wt%, respectively. The photo-resin was stirred for a few minutes using a magnet stirrer.

Fabrication of SWCNT/Polymer Composite: A Ti:sapphire femtosecond pulsed laser (Tsunami, Spectra Physics Newport Corp.), with a wavelength of 780 nm, a pulse width of 100 fs, and a repetition rate of 82 MHz, was used as the light source. The laser beam was focused by an oil-immersion objective lens (100x, NA 1.4, Zeiss) onto the SWCNT-dispersed photo-resin casted on a glass substrate placed on a three dimensional piezoelectric stage. The stage moved the resin relative to the focus spot according to programmed patterns. Arbitrary structures were created following the trajectory of the focus spot. The spatial resolution for fabrication was tuned by changing the incident laser intensity, and the typical laser intensity used in this study was ca. 25 mW/μm^2. The laser scanning speed was kept constant at 5 nm/ms.

The Orientation Direction and Strength of Alignment of SWCNTs Measurements with Polarized Raman Microspectroscopy: Polarized Raman microspectroscopy experiments were conducted using a Raman microscope (Raman-11, Nanophoton Corp.). The excitation laser beam, with a wavelength of 785 nm, was polarized after passing through a polarizer, and focused onto a sample through an objective lens (100x, NA 0.9). The polarization direction was controlled with a half-wave plate placed between the objective lens and the polarizer. Raman scattering was collected with the same objective lens, and the polarization direction was rotated to be the same as that of the incident light after passing through the half-wave plate. The laser intensity and exposure time were optimized to take Raman spectra with a sufficient signal-to-noise ratio. The polarized Raman intensity depends on the polarization angle, θ, of the incident laser beam, and the angular dependence of the Raman peak intensity, $I(\theta)$, is fitted with the following function:[32,33]

$$I(\theta) \propto \left(\frac{6}{7}cos^2\theta - \frac{2}{7}\right)\langle P_2(cos\theta)\rangle + \left(cos^4\theta - \frac{6}{7}cos^2\theta + \frac{3}{35}\right)\langle P_4(cos\theta)\rangle + \frac{1}{5} \quad (1)$$

where $<P_2(\cos\theta)>$ and $<P_4(\cos\theta)>$ are the second- and forth-order orientation parameters, respectively. $<P_2(\cos\theta)>$ is specifically known as the nematc order parameter, *S*, which is equal to 1 for perfect alignment and 0 for complete random orientations.

Experimental Apparatus: SEM observations were made using a Field Emission-Scanning Electron Microscope (FE-SEM, JSM-6330F, JEOL). Before SEM observation, the sample was Osmium-coated with a thickness of a few nm using an Osmium-coater (HPC-30W, Vacuum Device Inc.).

Acknowledgements

This research is supported by The Canon Foundation, and KAKENHI Grant-in-Aid for Young Scientists (No. 21686010, 19810012), MEXT, Japan. J.K. acknowledges financial support from the U.S. National Science Foundation (through Grant No. OISE-0968405), the Department of Energy (through Grant No. DE-FG02–06ER46308), and the Robert A. Welch Foundation (through Grant No. C-1509).

Received: February 18, 2014
Revised: May 1, 2014
Published online: June 18, 2014

[1] L. Ci, J. Suhr, V. Pushparaj, X. Zhang, P. M. Ajayan, *Nano Lett.* **2008**, *8*, 2762.
[2] F. Du, J. E. Fischer, K. I. Winey, *Phys. Rev. B* **2005**, *72*, 121404.
[3] I. Ivanov, G. E. Puretzky, H. Wang, Z. Pan, H. Cui, R. Jin, J. Howe, D. B. Geohegan, *Appl. Phys. Lett.* **2006**, *89*, 223110.
[4] J. Hone, M. C. Llaguno, M. Nemes, A. T. Johnson, J. E. Fischer, D. A. Walters, M. J. Casavant, J. Schmidt, R. E. Smalley, *Appl. Phys. Lett.* **2000**, *77*, 666.
[5] S. Shoji, H. Suzuki, R. P. Zaccaria, Z. Sekkat, S. Kawata, *Phys. Rev. B* **2008**, *77*, 153407.
[6] L. Ding, D. Yuan, J. Liu, *J. Am. Chem. Soc.* **2008**, *130*, 5428.
[7] W. Z. Li, S. S. Xie, L. X. Qian, B. H. Chang, B. S. Zou, W. Y. Zhou, R. A. Zhao, G. Wang, *Science* **1996**, *274*, 1701.
[8] F. Ko, Y. Gogotsi, A. Ali, N. Naguib, H. Ye, G. Yang, C. Li, P. Willis, *Adv. Mater.* **2003**, *15*, 1161.
[9] N. Behabtu, C. C. Young, D. E. Tsentalovich, O. Kleinerman, X. Wang, A. W. K. Ma, E. A. Bengio, R. F. Waarbeek, J. J. Jong, R. E. Hoogerwerf, S. B. Fairchild, J. B. Ferguson, B. Maruyama, J. Kono, Y. Talmon, Y. Cohen, M. J. Otto, M. Pasquali, *Science* **2013**, *339*, 182.
[10] C. L. Pint, Y. Q. Xu, S. Moghazy, T. Cherukuri, N. T. Alvarez, E. H. Hároz, S. Mahzooni, S. K. Doorn, J. Kono, M. Pasquali, R. H. Hauge, *ACS Nano* **2010**, *4*, 1131.
[11] P. M. Ajayan, O. Stephan, C. Colliex, D. Trauth, *Science* **1994**, *265*, 1212.
[12] S. Nanot, A. W. Cummings, C. L. Pint, A. Ikeuchi, T. Akiho, K. Sueoka, R. H. Houge, F. Léonard, J. Kono, *Sci. Rep.* **2013**, *3*, 1335.
[13] L. Ren, C. L. Pint, L. G. Booshehri, W. D. Rice, W. Wang, D. J. Hilton, K. Takeya, I. Kawayama, M. Tonouchi, R. H. Hauge, J. Kono, *Nano Lett.* **2009**, *9*, 2610.
[14] S. V. Ahir, E. M. Terentjev, *Nat. Mater.* **2005**, *4*, 491.
[15] H. Butt, Q. Dai, R. Rajesekharan, T. Wilkinson, G. Amaratunga, *ACS Nano* **2011**, *5*, 9138.
[16] Y. L. Zhang, Q. D. Chen, H. Xia, H. B. Sun, *Nano Today* **2010**, *5*, 435.
[17] B. B. Xu, Y. L. Zhang, H. Xia, W. F. Dong, H. Ding, H. B. Sun, *Lab Chip* **2013**, *13*, 1677.
[18] L. Li, R. R. Gattass, E. Gershgoren, H. Hwang, J. T. Fourkas, *Science* **2009**, *324*, 910.
[19] Z. Gan, Y. Cao, R. A. Evans, M. Gu, *Nat. Commun.* **2013**, *4*, 2061.
[20] S. Maruo, O. Nakamura, S. Kawata, *Opt. Lett.* **1997**, *22*, 132.
[21] S. Kawata, H. B. Sun, T. Tanaka, K. Takada, *Nature* **2001**, *412*, 697.
[22] M. Deubel, G. V. Freymann, M. Wegener, S. Pereira, K. Busch, C. M. Soukoulis, *Nat. Mater.* **2004**, *3*, 444.
[23] A. Ledermann, L. Cademartiri, M. Hermatschweiler, C. Toninelli, G. A. Ozin, D. S. Wiersma, M. Wegener, G. V. Freymann, *Nat. Mater.* **2006**, *5*, 942.
[24] T. Ergin, N. Stenger, P. Brenner, J. Pendry, M. Wegener, *Science* **2010**, *328*, 337.
[25] M. Kadic, T. Bückmann, N. Stenger, M. Thiel, M. Wegener, *Appl. Phys. Lett.* **2012**, *100*, 191901.
[26] S. Maruo, K. Ikuta, H. Korogi, *Appl. Phys. Lett.* **2003**, *82*, 133.
[27] H. Ishitobi, S. Shoji, T. Hiramatsu, H. B. Sun, Z. Sekkat, S. Kawata, *Opt. Exp.* **2008**, *16*, 14106.
[28] Z. B. Sun, X. Z. Dong, W. Q. Chen, S. Nakanishi, X. M. Duan, S. Kawata, *Adv. Mater.* **2008**, *20*, 914.
[29] K. Masui, S. Shoji, K. Asaba, T. C. Rodgers, F. Jin, X. M. Duan, S. Kawata, *Opt. Exp.* **2011**, *19*, 22786.
[30] H. Xia, J. Wang, Y. Tian, Q. D. Chen, X. B. Du, Y. L. Zhang, Y. He, H. B. Sun, *Adv. Mater.* **2010**, *22*, 3204.
[31] S. Ushiba, S. Shoji, K. Masui, P. Kuray, J. Kono, S. Kawata, *Carbon* **2013**, *59*, 283.
[32] J. Shaver, A. N. G. Parra-Vasquez, S. Hansel, O. Portugall, C. H. Mielke, M. Ortenberg, R. H. Hauge, M. Pasquali, J. Kono, *ACS Nano* **2009**, *3*, 131.
[33] T. Liu, S. Kumar, *Chem. Phys. Lett.* **2003**, *378*, 257.
[34] K. Takada, D. Wu, Q. D. Chen, S. Shoji, H. Xia, S. Kawata, H. B. Sun, *Opt. Lett.* **2009**, *34*, 566.
[35] F. Borghase, P. Denti, R. Saija, M. A. Itaì, O. M. Maragò, *Phys. Rev. Lett.* **2008**, *100*, 163903.
[36] J. Do, M. Fedoruk, F. Jäckel, J. Feldmann, *Nano Lett.* **2013**, *13*, 4164.